5- Mohr-Coulomb Material Model

Mohr-Coulomb model is the most common model in the context of geomaterials and in particular soils (e.g. Owen and Hinton 1980, Pietruszczak 2010). The specification of this model and its yield criterion typically involves Coulomb's hypothesis, which postulated a linear relationship between shear strength on a plane and the normal stress acting on it

$$\tau = c - \sigma_n \tan \varphi \tag{5.1}$$

where τ is the shear strength, σ_n is the normal stress (tension positive), φ is in the angle of internal friction and c is the cohesion.

The mechanical behavior of a material that is modelled with Mohr-Coulomb model includes features such as:

- Isotropic shear strength (peak and residual) that has cohesive-frictional characteristic, and increases linearly with the level of stress/confinement

- Tensile strength (by using a tension cutoff yield function)

- Dilation (increase in volume) or critical state (constant volume) at failure

- Dependency of shear strength on Lode's angle (observed for most geomaterials)

The model is well suited for evaluation of stability of geotechnical/mining problems that does not include wide ranges of stress/confinement. Using the Shear Strength Reduction (SSR) method this model can evaluate safety factors equivalent to those calculated based on limit equilibrium approach (Slide), and in some cases provide better prediction of the failure modes and the safety factors. It can be also used with success for calculations of load-displacement in simulations that include geomaterials such as gravels, sands and rocks.

Combining the Coulomb criterion with Mohr circle representation of stress state and considering the admissible states the Mohr-Coulomb failure criterion in terms of principal stresses can be expressed as

$$F_s = \frac{1}{2}(\sigma_1 - \sigma_3) + \frac{1}{2}(\sigma_1 + \sigma_3)\, sin\, \varphi - c\, cos\, \varphi = 0 \tag{5.2}$$

In terms of stress invariants, the Mohr Coulomb yield surface is

$$F_s = \frac{I_1}{3} sin(\phi) + \sqrt{J_2}\left[cos(\theta) - \frac{1}{\sqrt{3}} sin(\theta)\, sin(\phi)\right] - c\, cos(\phi) = 0 \tag{5.3}$$

Or in other stress invariants terms

$$F_s = q + Mp - Nc = 0 \tag{5.4}$$

where

$$M = \frac{3 \sin \varphi}{\sqrt{3} \cos \theta - \sin \theta \sin \varphi} \quad , \quad N = \frac{3 \cos \varphi}{\sqrt{3} \cos \theta - \sin \theta \sin \varphi} \tag{5.5}$$

RS[2] and RS[3] accept peak values and residual values for the cohesion and friction angle. This means that after the initial yielding the strength of the material instantly drops from its peak state to a lower residual state. The Mohr-Coulomb model in RS[2] and RS[3] is an elasto-brittle-plastic material model in general. In the case where the residual values are the same as peak values the behavior is elasto-perfect-plastic.

The plastic potential function has the same from as the yield surface

$$Q_s = \frac{I_1}{3} \sin(\psi) + \sqrt{J_2} \left[\cos(\theta) - \frac{1}{\sqrt{3}} \sin(\theta) \sin(\psi) \right] = const. \tag{5.6}$$

where ψ is the dilation angle. This parameter should be less than or equal to the (residual) friction angle which makes the flow rule non-associated or associated respectively.

The dialog for defining this constitutive model is shown in Figure 5.1. Sample stress paths of drained and undrained triaxial compression tests that could be simulated with this model are presented in Figure 4.2 and 4.3. All the tests start form a hydrostatic confinement of $p = p' = 100$ kPa.

Stress paths of the drained tests include variations of axial stress and volumetric strain with increasing axial strain, variation of deviatoric stress with deviatoric strain and the stress path in p-q plane. The yield surface is also shown in the p-q plane. The simulated behavior is an elasto-perfect plastic behavior. The dilation effect is illustrated in the variation of volumetric strain with axial strain.

Stress paths of the undrained tests include the variation of axial stress and pore water pressure with increasing axial strain, variation of deviatoric stress with deviatoric strain and the stress path in p-q plane. The yield surface is also shown in the p-q plane. The dilation effect is illustrated in the plot of the stress path in p-q plane that also include the yield surface. The generation of negative pore water pressure in material with dilation leads to the increase in the effective mean stress, as the stress path lays on the yield surface and follows it to higher levels of deviatoric stress.

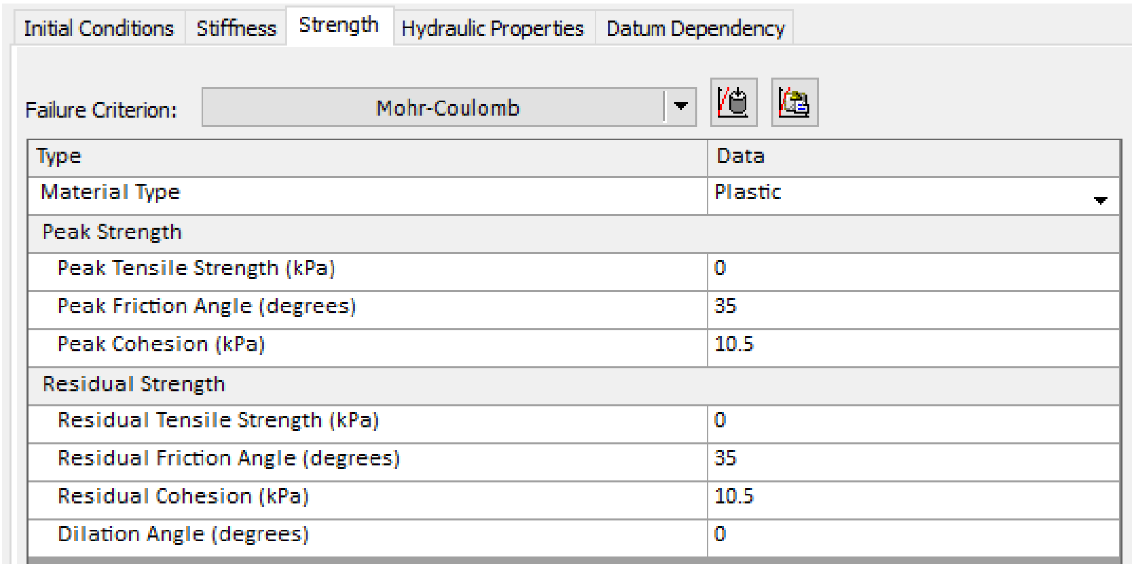

Figure 5.1. Dialog for defining Mohr-Coulomb model

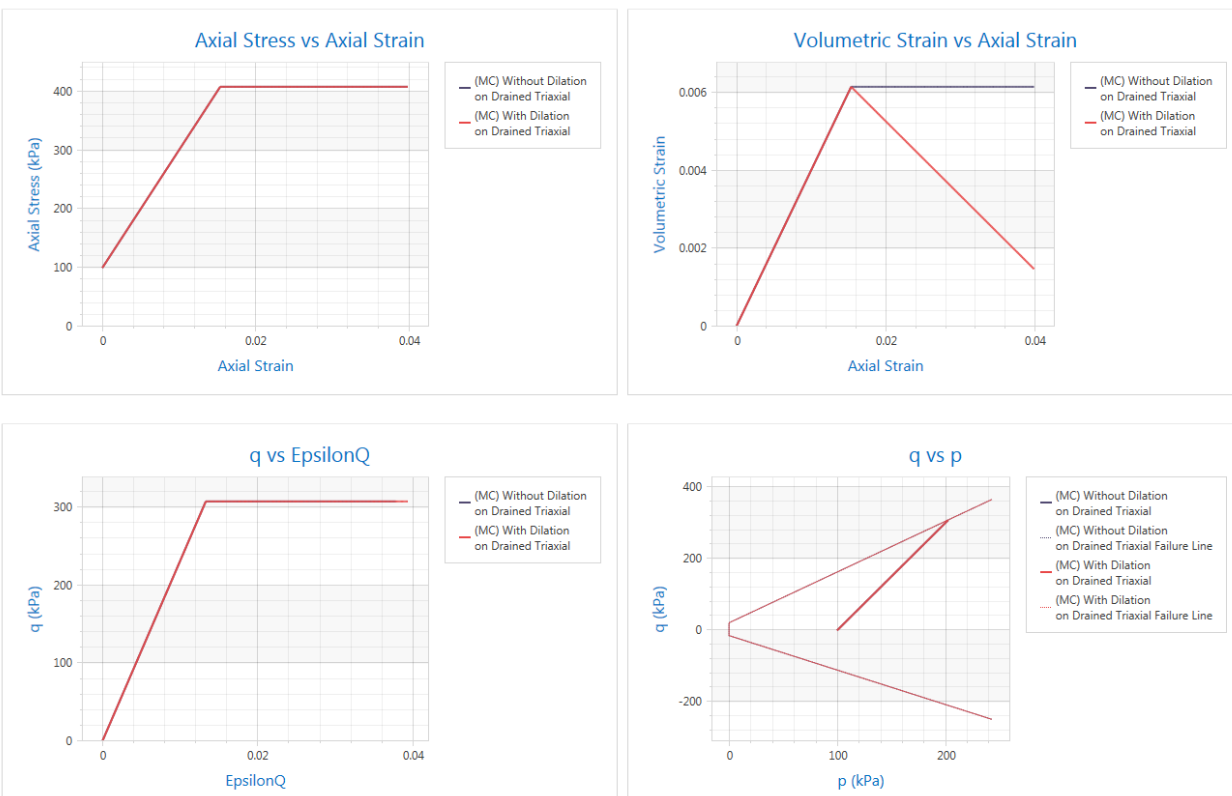

Figure 5.2. Stress paths of drained triaxial tests on materials with Mohr-Coulomb constitutive model

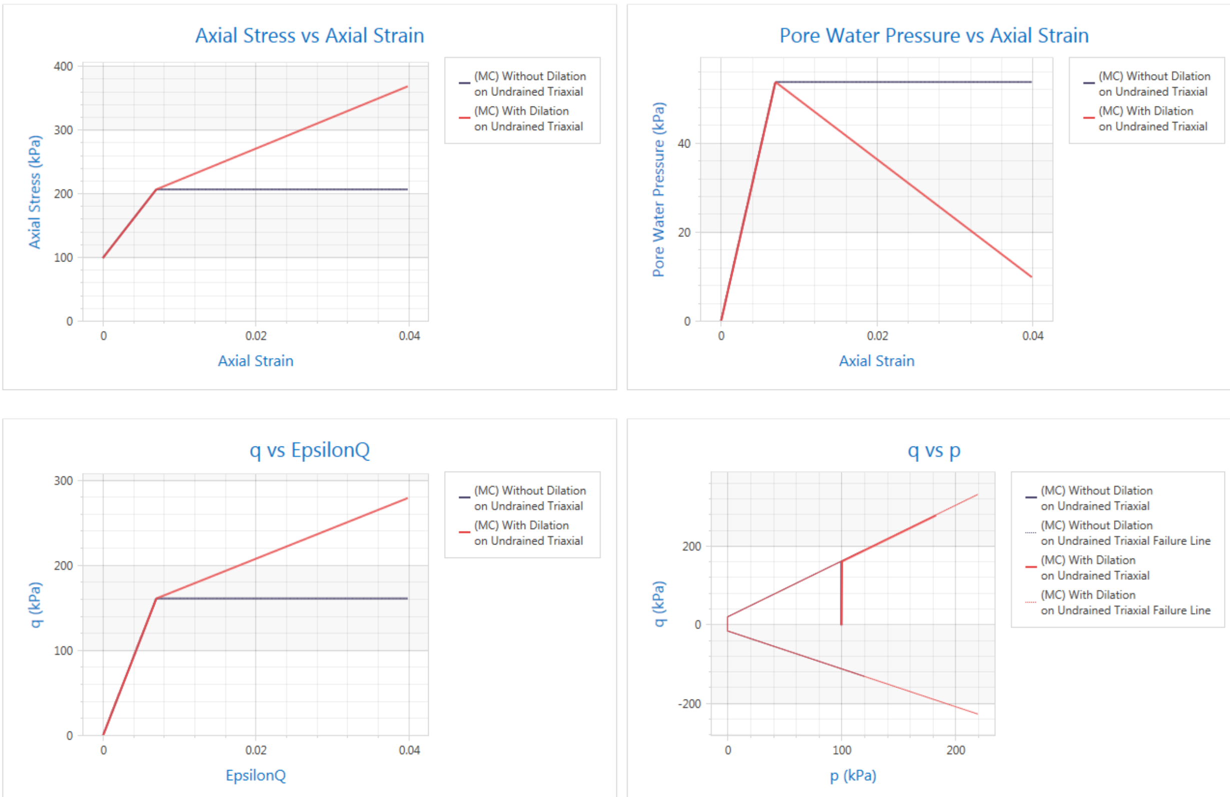

Figure 5.3. Stress paths of undrained triaxial tests on materials with Mohr-Coulomb constitutive model

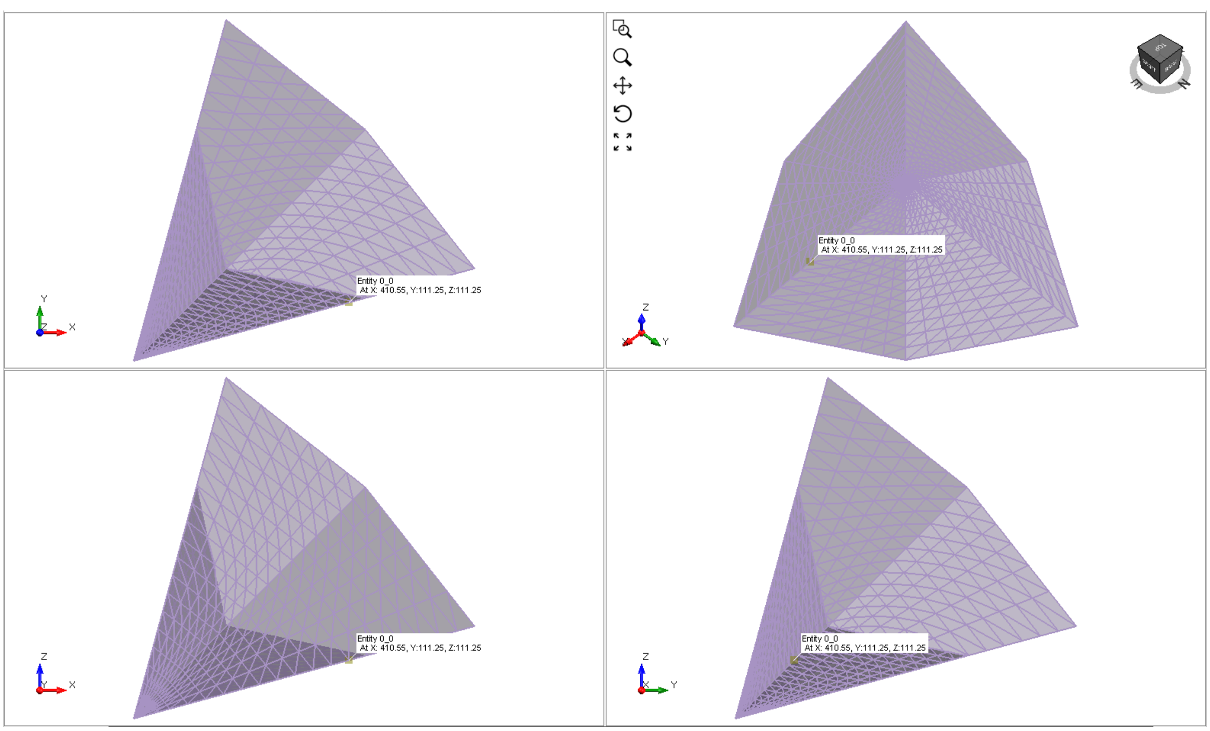

Figure 5.4. Yield surface of Mohr-Coulomb model in 3D stress space

The yield surface of this model is a line in 2D stress space as shown in Figures 5.2 and 5.3 and has an irregular hexagonal pyramid shape in 3D stress space as presented in Figures 5.4. The definition of yield surface includes the Lode's angle and thus the projection of this yield surface in Π plane, with normal direction being the stress space diagonal, deviates from the circular shape of Drucker-Prager model.

The model also accept a tension cutoff. The yield surface of the tension cut off is

$$F_T = \sigma_1 - T = 0 \tag{5.7}$$

In above T is the tensile strength of the material. The flow rule for tensile failure is associated.

In slope stability analysis using the Finite Element Method with Shear Strength Reduction, the factored shear strength can be calculated by applying the Strength Reduction Factor the shear strength defined in equation (5.1)

$$\frac{\tau}{SRF} = \frac{c - \sigma_n \tan\varphi}{SRF} \tag{5.8}$$

The factored Mohr Coulomb properties after the application of SRF are

$$c_{SRF} = \frac{c}{SRF} \ , \quad \varphi_{SRF} = \operatorname{atan}\left(\frac{\tan\varphi}{SRF}\right) \tag{5.9}$$

The SRF is applied to the dilation angle in the same way that is applied to the friction angle.

References

Dawson, E.M., Roth, W.H. and Drescher, A. (1999), Slope stability analysis by strength reduction, Geotechnique, vol. 49, no. 6, pp. 835-840.

Duncan, J.M. (1996), State of the art: limit equilibrium and finite-element analysis of slopes, Journal of Geotechnical Engineering, vol. 122, no. 7, pp. 577-596.

Griffiths, D.V. and Lane, P.A. (1999), Slope stability analysis by finite elements, Geotechnique, vol. 49, no. 3, pp. 387-403.

Owen D.R.J. and Hinton E. (1980), Finite Elements in Plasticity- Theory and Practice Pineridge Press, Swansea.

Pietruszczak, S. (2010). Fundamentals of Plasticity in Geomechanics. CRC Press.